Modeling the OH-Initiated Oxidation of Mercury in the Global Atmosphere Without Violating Physical Laws

Theodore S. Dibble^{a*}, Hanna L. Tetu^a, and Yuge Jiao^a, Colin P. Thackray^b, Daniel J. Jacob^{b, c}

- a) Department of Chemistry, State University of New York, College of Environmental Science and Forestry, 1 Forestry Drive, Syracuse, NY, 13210
- b) Harvard John A. Paulson School of Engineering and Applied Sciences, Harvard University, Cambridge, MA, USA
 - c) Department of Earth & Planetary Sciences, Harvard University, Cambridge, MA, USA

ABSTRACT

In 2005, Calvert and Lindberg (Calvert, J. G.; Lindberg, S. E. Atmos. Environ. 2005, 39, 3355–3367) wrote that the use of laboratory-derived rate constants for OH + Hg(0) "...to determine the extent of Hg removal by OH in the troposphere will greatly over-estimate the importance of Hg removal by this reaction." The HOHg• intermediate formed from OH + Hg will mostly fall apart in the atmosphere before it can react. By contrast, in laboratory experiments, Calvert and Lindberg expected HOHg• to react with radicals (whose concentrations are much higher than in the atmosphere). Yet almost all models of oxidation of Hg(0) ignore the argument of Calvert and Lindberg. We present a way for modelers to include the OH + Hg reaction while accounting quantitatively for the dissociation of HOHg. We use high levels of quantum chemistry to establish the HO-Hg bond energy as 11.0 kcal/mole, and calculate the equilibrium constant for OH + Hg = HOHg•. Using the measured rate constant for association of OH with Hg, we determine the rate constant for HOHg• dissociation. Theory is also used to demonstrate that HOHg• forms stable compounds, HOHgY, with atmospheric radicals (Y = NO₂, HOO•, CH3OO•, and BrO). We then present rate constants for use in in modeling OH-initiated oxidation of Hg(0). We use this mechanism to model the global oxidation of Hg(0) in the period 2013-2015 using the GEOS-Chem 3D model of atmospheric chemistry. Because of the rapid dissociation of HOHg•, OH accounts for <1% of the global oxidation of Hg(0) to Hg(II), while Br atoms account for 97%.

*Corresponding Author: tsdibble@esf.edu

INTRODUCTION

The toxicity of mercury motivates research into its environmental chemistry and transport. It has long been realized that the atmosphere enables transport of mercury from emission sites to anywhere in the globe. Recently, the international community agreed to reduce emissions of mercury in order to reduce harm to humans and the environment. This agreement, the Minimata Convention, calls for modeling of mercury fate and transport in order to guide emissions reductions.²

Gaseous elemental mercury (Hg(0), aka GEM) dominates mercury emissions to the atmosphere.³ GEM is oxidized in the atmosphere to mercuric compounds (Hg(II)), which are soluble in water and, hence, efficiently removed by deposition.¹ As a result, understanding the mechanism and kinetics of oxidation of Hg(0) is critically important for predicting when and where mercury enters ecosystems.^{4, 5} Yet the scientific community cannot agree on which species initiate the oxidation of GEM!^{6,7} This disagreement hinders the progress of research into the global cycling of mercury.

The hydroxyl radical (OH) is the most important oxidant for most organic and inorganic compounds in the atmosphere, so it is natural to suspect that it plays a major role in GEM oxidation. The reaction of OH with Hg is presumed to proceed via:

$$OH + Hg (+M) = HOHg \cdot (+M)$$
 (1)

where M is a third body. The three experimental studies of the kinetics of reaction (1) all agree well with each other; we summarize them here. Sommar et al. used a relative rate technique to obtain $k_1 = (8.7 \pm 3) \times 10^{-14}$ cm³ molecule⁻¹ sec⁻¹ at 295 K in 1 atm of air.⁸ Bauer et al reported an upper limit of 1.2×10^{-13} cm³ molecule⁻¹ sec⁻¹ at 298 K in 400 Torr of air using laser-induced fluorescence (LIF) detection of OH in the presence of excess Hg(0).⁹ Pal and Ariya used relative rate measurements to determine the rate constant as a function of temperature (283 K $\leq T \leq$ 353 K) in 1 atm air.¹⁰ At 295 K, their Arrhenius expression corresponds to a value only 10% higher than that of Sommar et al.

Subsequently, in 2005, Goodsite et al.¹¹ used computational chemistry to study the dissociation of HOHg•. They pointed out that the weak HO-Hg bond (they reported $D_0 = 9.4$ kcal/mole) would lead to fast dissociation of HOHg•. On account of this fast dissociation, they largely discounted the importance of OH radical in Hg(0) oxidation in favor of oxidation by Br atoms.

Calvert and Lindberg¹² tried to reconcile the fast dissociation of HOHg• with the results of the relative rate experiments. They pointed out that the high concentrations of radicals, •Y, in those experiments would enable HOHg• to react with radicals to make stable Hg(II) compounds via:

$$HOHg \bullet + \bullet Y + M \rightarrow HOHgY + M$$
 (2)

in competition with HOHg• dissociation. They concluded that OH-initiated oxidation of GEM would be much less efficient in the atmosphere than implied by experiments, due to the much lower radical concentrations in the atmosphere. As of this writing, their paper has been cited approximately 200 times, and that of Goodsite et al. has been cited over 250 times, yet almost all models of Hg(0) oxidation that include OH-initiation assume that the OH + Hg reaction is irreversible. This assumption violates detailed balancing.

How do models of the OH-initiated oxidation of GEM reconcile their assumption that reaction (1) is irreversible with the results of Goodsite et al. and Calvert and Lindberg? Some models ignore the issue by using operational definitions of the products rather than specifying their identity.^{13,14} In other instances the assumed irreversibility of reaction (1) is rationalized^{8,10,15} by the rapid occurrence of:

$$HOHg \bullet + O_2 + M \rightarrow HgO + HOO + M$$
 (3)

However, we know now that reaction (3) cannot occur under atmospheric conditions, because it is endothermic by ~60 kcal/mole. This endothermicity largely arises from the very low bond energy of HgO (~4 kcal/mole). Furthermore, as a result of its weak bonding, the HgO molecule will fall apart extremely rapidly:

$$HgO + M \rightarrow Hg + O + M$$
 (4)

As a result of reaction (4), the occurrence of reaction (1) followed by reaction (3) cannot account for the loss of Hg(0) observed in the presence of OH without violating the law of mass conservation. While the last several years have seen extensive studies of the kinetics and mechanism of Br-initiated oxidation of Hg(0), $^{18,21-28}$ similar work has not been carried out for OH-initiated oxidation.

The importance of OH in initiating Hg(0) oxidation depends, in large part, on the rate of HOHg• dissociation and the rate of oxidation of HOHg• to Hg(II) compounds. The rate of HOHg• dissociation has not been determined experimentally, and depends sensitively on the HO-Hg bond energy. We start by using quantum chemistry to determine the HO-Hg bond dissociation energy with high precision. We also show that the HHgO• isomer of HOHg• will not form from OH + Hg. Using standard methods of statistical mechanics we then obtain the equilibrium constant, $K_1(T)$, for HO-Hg formation in reaction (1). Together with the experimental measurements of $k_1(T)$, this enables determination of the rate constant, $k_{-1}(T)$, for HOHg• dissociation. Following this, we use quantum chemistry to demonstrate that HOHg•, like BrHg•, 24,29 forms thermally stable molecules in addition reactions with NO2, HOO, CH3OO, and BrO:

$$HOHg \bullet + NO_2 + M \rightarrow HOHgONO$$
 (and isomers) $+ M$ (2a)

$$HOHg \bullet + HOO \bullet + M \rightarrow HOHgOOH + M$$
 (2b)

$$HOHg \bullet + CH_3OO \bullet + M \rightarrow HOHgOOCH_3 + M$$
 (2c)

$$HOHg \bullet + BrO \bullet + M \rightarrow HOHgOBr + M$$
 (2d)

Also like BrHg•, HOHg• binds rather weakly to O₂ and NO:

$$HOHg \bullet + O_2 + M = HOHgOO \bullet + M$$
 (2e)

$$HOHg \bullet + NO + M = HOHgNO + M$$
 (2f)

such that dissociation of HOHgOO• and HOHgNO occurs more rapidly than they could undergo other reactions. Next, we present arguments that HOHg• will not abstract hydrogen atoms from volatile organic compounds (VOCs) and will not add efficiently to alkenes. We then use the parallels between the HOHg-Y and BrHg-Y bond energies to suggest a set of rate constants for use in modeling the OH-initiated oxidation of Hg(0). Finally, we present results of modeling of the effect of OH-initiated oxidation of Hg(0) on global mercury concentrations.

METHODS

Calculations on HOHg-Y compounds used Gaussian 09^{30} and Gaussian $16.^{31}$ Spin-unrestricted methods were used for open-shell molecules except as noted. The standard Dunning (aug-)cc-pVXZ³² (X = D, T, Q, or 5) basis sets were used for O and H. To account for scalar relativistic effects, we used the Stuttgart/Cologne scalar pseudopotentials for the 60 innermost electrons of Hg (ECPMDF60). The corresponding (aug)-cc-pVXZ basis sets of Peterson and co-workers for electrons outside this ECP. 33,35,36 Hereafter, we refer to this combination of pseudopotentials and basis sets as VXZ or AVXZ (when augmented with diffuse functions). Where not otherwise specified, post-Hartree-Fock methods correlated only the 5d and 6s electrons of Hg, the 4s and 4p electrons of Br, and the valence electrons of H, C, N, and O.

Calculations to determine HOHg-Y bond energies and the relative energy of HOHg• and its HHgO• isomer were carried out using geometries and unscaled harmonic vibrational frequencies (and zero-point energies) computed at PBE0/AVTZ. These calculations used a pruned grid of 99 radial shells with 590 angular points per shell. This level of theory has proven to do a good job for structure and vibrational frequencies of the analogous BrHgY species. Energies were recalculated at CCSD(T)/AVTZ.

The HO-Hg bond energy was determined by a composite method similar to the HEAT345-(Q) protocol. ^{37,38} Coupled-cluster calculations used CFOUR Beta v2.0³⁹, except that UHF-CCSDT(Q) calculations were done by MRCC codes. ⁴⁰ RASSI/CASPT2 calculations were carried using Molcas 8.0. ⁴¹ First, the geometries of OH and HOHg• were optimized at CCSD(T) with AVTZ and AVQZ basis sets using analytical gradients. ⁴² Harmonic vibrational frequencies were calculated at CCSD(T)/AVTZ. Geometries were reoptimized using the analogous valence basis sets designed for correlating all electrons not included in the ECP. ^{36,43} We denote this combination of basis sets and pseudopotentials as AwCVTZ. We determined core-valence effect on geometry, ΔCV, from the difference between geometric parameters computed at CCSD(T)/AVTZ versus CCSD(T,Full)/AwCVTZ.

Absolute energies were refined at the CCSD(T)/AVQZ+ Δ CV geometries. CCSD(T) energies with all electrons correlated were extrapolated to the complete basis set (CBS) limit using CCSD(T)/AwCVXZ energies for X=3 (T), 4 (Q), and 5 by fitting to the formula:^{44,45}

$$E(n) = E_{CBS} + Be^{-(n-1)} + Ce^{-(n-1)^2}$$
(5)

These CCSD(T,Full)/CBS energies were used to obtain an initial value of the zero-point energy-exclusive bond energy at 0 K (D_{e,CBS}). As described below, correction terms to this value of D_e were added to account for the full triples excitations, a perturbative estimate of the quadruple excitations, and spin orbit coupling.

The effect, ΔT , of the difference between the perturbative estimate of the triples excitation and its exact expresssion^{46,47} was determined by taking the difference between D_e computed at CCSDT/VTZ and CCSD(T)/VTZ:

$$\Delta T = D_{e,CCSDT/VTZ} - D_{e,CCSD(T)/VTZ}$$
(6)

The corrections for the noniterative quadruple excitation^{48,49} ($\Delta(Q)$) were applied by comparing CCSDT(Q)/VDZ energies and CCSDT/VDZ energies as:

$$\Delta(Q) = D_{e,CCSDT(Q)/VDZ} - D_{e,CCSDT/VDZ}$$
(7)

The correction for spin-orbit coupling (Δ SOC) was computed using the restricted active space state interaction (RASSI) method^{50,51} with complete active space second-order perturbation theory (CASPT2)^{52,53} using the atomic mean field integral (AMFI)⁵⁴ algorithm. The DK2 Hamiltonian was used in conjunction with relativistic RCC-ANO basis sets.^{55,56} The active space includes the 6s and 6p orbitals for Hg and the 2s and 2p orbitals for O. This approach yields a zero-field splitting for OH radical of 148 cm⁻¹, which agrees well with the experimental value of 139.2 cm⁻¹.⁵⁷ Expanding the active space from (5e,60) to (7e,70) lowered this zero-field splitting by only 1.5 cm⁻¹, suggesting that increasing the size of the active space would not significantly improve the accuracy of the calculation. Subtracting the reaction energy of the lowest spin-free (SF) state from that of the lowest spin-orbit (SO) state yields Δ SOC:

$$\Delta SOC = D_{e,SO-RASSI/ANO-RCC} - D_{e,SF-RASSI/ANO-CC}$$
(8)

Zero-point energies (ZPEs) of OH and HOHg• were computed at CCSD(T)/AVTZ. The final value of the bond energy, D₀, was computed as:

$$D_0 = D_{e,CBS} + \Delta T + \Delta(Q) + \Delta SOC + \Delta ZPE$$
 (9)

Results and Discussion

OH + Hg = HOHg•. Figure 1 displays the geometry of HOHg• and Table 1 compares the present results with previous theoretical results. The structure is rather sensitive to the method and basis set employed. Note that the CCSD(T)/AVQZ structure of Saiz-Lopez et al. ²⁶ is very close to that reported here (Hg-O distance shorter by 0.007 Å), but rather different from the geometry they

reported using MRCISD+Q. The H-O bond distance is 0.0037 Å smaller in HOHg• than in the OH radical at the CCSD(T)/AVQZ + Δ CV level of theory. Table 2 lists the harmonic vibrational frequencies and band intensities of HOHg•, in which the frequency of the O-H stretch mode is only 31 cm⁻¹ larger than in the OH radical. These small differences in structure and vibrational frequency between OH radical and the OH group of HOHg• do not reflect the large change in electronic structure upon addition of Hg to OH: both the Mulliken and Hirshfeld population analyses assign over half the spin density in HOHg• to the mercury atom.

Table 1. Structural parameters of HOHg• (²A') reported in several studies (distances, R, in Ångstroms and angle, A, in degrees).

Method	R(H-O)	R(O-Hg)	A(HOHg)	Ref.
B3LYP/CEP-121G	0.99	2.25	106.8	11
B3LYP/AVTZ ^a	0.9690	2.2079	103.6	58
B3LYP/ZORA-GI/NESC ^b	-	2.181		20
M06-2X/AVTZ	0.964	2.100	106.2	59
MRCISD+Q/aug-cc-pVQZ	0.9433	2.1342	106.9	26
$CCSD(T,Full)/AwCVTZ + \Delta CV$	0.9662	2.1031	103.88	this work

a) using ECP60MWB

b) using a triple- ζ basis set

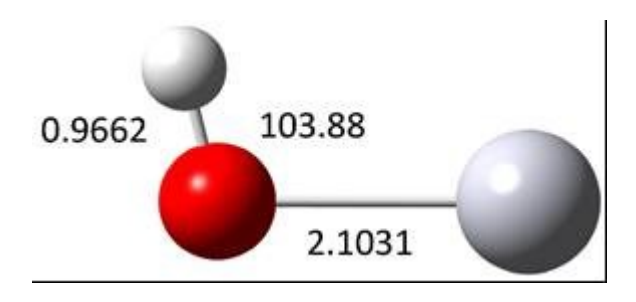


Figure 1. Geometry (bond distances in Å and bond angles in degrees) of HOHg• (2 A') at CCSD(T,Full)/AwCVTZ+ Δ CV.

Table 2. Vibrational mode descriptions, harmonic frequencies (v, cm⁻¹), and integrated absorption intensities (S, km/mol) for HOHg• at CCSD(T)/AVTZ.

mode	ν	S
HgO stretch	401.4	10.2
HOHg bend	824.0	45.0
OH stretch	3749	42.0

Table 3 lists the various contributions to the HO-Hg bond energy (D₀). Note that the extrapolation of CCSD(T,Full) energies from AwCV5Z to the CBS limit changes the bond energy by only 0.18 kcal/mole. The other correction terms are also small, which encourages us to believe that the final result is very accurate. The T_1 diagnostic⁶⁰ for HOHg• is only 0.020, which is consistent with the modest effects we observe when extending the coupled cluster calculations past the perturbative estimate of the triples correction. As can be seen from Table 3, the sum of the ΔT + Δ (Q) + Δ SOC terms is quite small.

Table 3. Contributions to the HO-Hg bond energy (kcal/mol).

Term	Value
CCSD(T,Full)/CBS	12.45
ΔT	0.14
$\Delta(Q)$	0.32
$\Delta \mathrm{SOC}$	-0.10
ΔZPE (harmonic)	-1.80
Total	11.02

The HEAT345-(Q) method, which is similar to the approach used here, has an uncertainty of about 0.2 kcal/mol for bond energies of diatomic molecules in the first two rows of the periodic table.^{37,38,61} As discussed elsewhere, there are no benchmarks for HEAT345-(Q) for mercury compounds.⁶² HEAT345-(Q) includes a correction for the diagonal Born-Oppenheimer approximation. Because the bond being formed in reaction (1) is between two non-hydrogen atoms, we expect this correction to be negligible here. We estimate our value of D₀ to have an uncertainty (2 s.d.) of about 0.4 kcal/mole; this assessment relies on the small size of the corrections to the CCSD(T,Full)/CBS energies seen in Table 3 and the high accuracy expected of the CCSD(T,Full)/AwCVTZ geometry and CCSD(T)/AVTZ harmonic frequencies.

Goodsite et al.¹¹ and Ezarfi et al.⁵⁸ obtained somewhat lower values of D₀ than we did (9.0 and 9.5 kcal/mole, respectively). They both used a low level of theory (B3LYP), so the discrepancy between their values and ours is understandable. Cremer et al. used explicitly relativistic calculations with a basis set that was triple-zeta quality; they computed CCSD(T) energies at a B3LYP geometry.²⁰ Their bond enthalpy of 12.4 kcal/mole at 298 K corresponds to D₀ of 11.4 kcal/mole, which agrees very well with our result. Tossell⁶³ reported D₀ of only 5.5 kcal/mole at CCSD(T)//CCD/SBK. Guzman and Bozzelli⁵⁹ reported a bond enthalpy of 14.1 kcal/mole at 298 K, corresponding to D₀ of 13.1 kcal/mole. Although their bond enthalpy was based on CCSD(T)/CBS energies, it relied on experimental values of the enthalpies of formation of mercury halides—values that possess uncertainties of at least 2 kcal/mole.⁶⁴ Note that one theoretical study reported the unphysical result that HOHg• was unstable by 21 kcal/mole with respect to OH + Hg.⁶⁵

Recall that the product of OH + Hg has not been determined experimentally. Conceivably, this reaction could produce HHgO•. Because HHgO• is an Hg(II) compound, formation of

HHgO• from OH + Hg would tend to invalidate the arguments of Calvert and Lindberg regarding the efficiency of OH-initiated oxidation of Hg(0). Note that, based on literature thermodynamics, ^{66,21} one can estimate that BrHgO• and ClHgO• are more stable than the corresponding BrO-Hg and ClO-Hg complexes by almost 20 kcal/mole. So we were somewhat surprised to find that HHgO• lies 37.7 (36.0) kcal/mol above HOHg• at the CCSD(T)//PBE0/AVTZ (PBE0/AVTZ) level of theory. Ezarfi et al. reported a similar energy difference (40.8 kcal/mole) at B3LYP/AVTZ. Given these results, we can conclude that HHgO• cannot be formed from OH + Hg.

Using the value of D_0 obtained here, together with literature data on Hg and OH (listed in the Supporting Information), we computed the equilibrium constant, $K_c(T)$, for reaction (1) at several temperatures over the range 200-320 K. These values can be fit with less than 2% error by the expression:

$$K_c = 2.74 \times 10^{-24} \,\mathrm{e}^{+5770/\mathrm{T}} \,\mathrm{cm}^3 \,\mathrm{molecule}^{-1}$$
 (10)

We now use $K_c(T)$ and $k_1(T)$ to determine the rate constant, $k_{-1}(T)$, for dissociation of HOHg. Pal and Ariya¹⁰ reported the bimolecular rate constant, k_1 , (T, 1 atm), for HOHg• formation as $3.55 \times 10^{-14} \text{ e}^{+294/\text{T}} \text{ cm}^3$ molecule⁻¹ sec⁻¹ at 1 atm of pressure. The rate constant will depend on the pressure. Given that the analogous reactions forming ClHg• and BrHg• appear to be in the low-pressure limit at pressures up to 600 Torr, 67,68 and given that the HO-Hg bond is significantly weaker than the bonds in ClHg• and BrHg•, 20 we assume that reaction (1) is also in the low-pressure limit. This implies that $k_1(T, 1 \text{ atm}) = k_{1,0}(T)[M]_{1\text{atm}}$, where $k_{1,0}(T)$ is the rate constant in the low-pressure limit and $[M]_{1\text{atm}}$ is the total number density of gas phase species at one atmosphere total pressure at the corresponding temperature. With this assumption, we can express the rate of reaction (1) as:

Rate =
$$k_{1,0}(T)[OH][Hg][M]$$
 (11)

We find $k_{1,0}(T)$, the termolecular association rate constant, to be:

$$k_1(T) = 3.34 \times 10^{-33} \text{ e}^{+43/\text{T}} \text{ cm}^6 \text{ molecule}^{-2} \text{ sec}^{-1}$$
 (12)

with error of less than 1.5% due to the fitting expression. The resulting bimolecular rate constant for dissociation of HOHg• is fit to within 4% by the expression:

$$k_{-1,0}(T) = 1.22 \times 10^{-9} \,\mathrm{e}^{-5720/\mathrm{T}} \,\mathrm{cm}^3 \,\mathrm{molecule}^{-1} \,\mathrm{sec}^{-1}$$
 (13)

where the rate of dissociation equals $k_{-1,0}(T)$ [HOHg•][M]. At 298 K and 1 atm, $k_{-1,0}$ [M] equals 140 sec⁻¹, corresponding to a lifetime of only 7 ms. This lifetime is significantly longer than the 0.3 ms computed by Goodsite et al., ¹¹ on account of our finding a stronger bond energy.

Bimolecular Reactions of HOHg• Figure 2 depicts the structures of the stable Hg(II) species that can be formed in reactions of HOHg• with various atmospherically abundant radicals (•Y). HOHg-Y distances are very similar to those computed for BrHg-Y at the same level of theory.²⁴ Paralleling our results for BrHg• + NO₂, interaction of HOHg• with NO₂ yields three isomers/conformers: HOHgNO₂, *anti*-HOHgONO, and *syn*-HOHgONO. Figure 3 depicts the

potential energy profile for the HOHg• + NO₂ system, including transition states for isomerization of HOHgNO₂ to *anti*-HOHgONO to *syn*-HOHgONO. Note that the HOHgO• + NO (not shown in Figure 3) lies 7 kcal/mole above HOHg• + NO₂ at CCSD(T)//PBE0/AVTZ, so HOHgO• + NO will not form from HOHg• + NO₂.

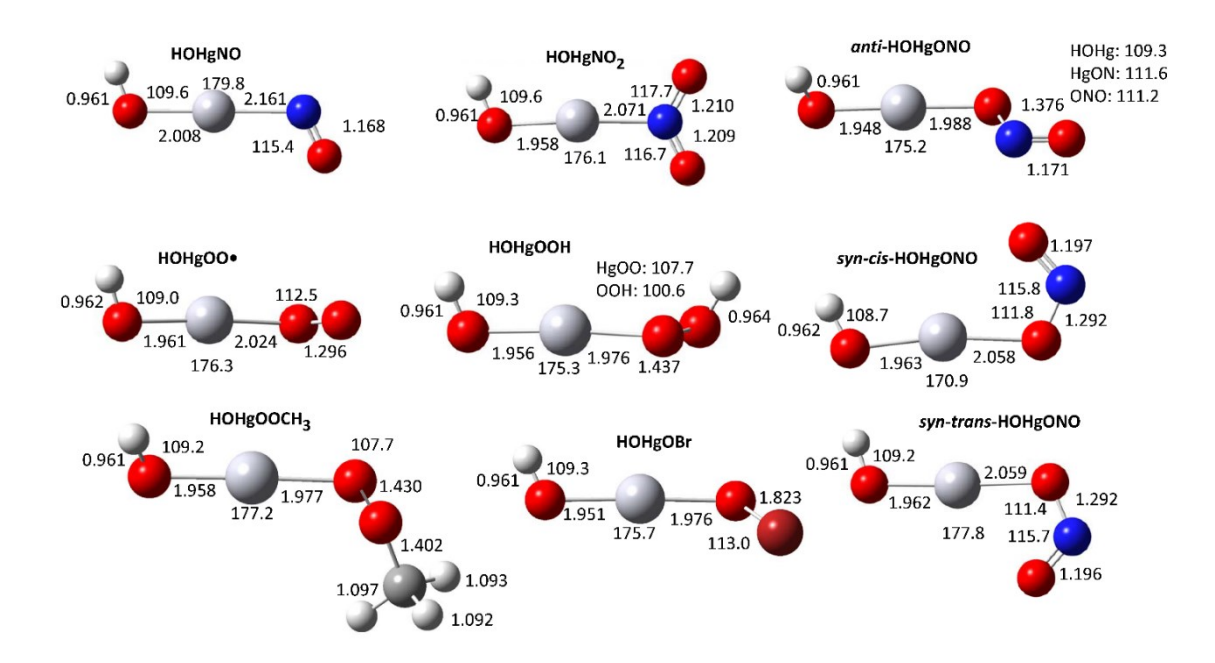


Figure 2. Structures of HOHgY compounds. Bond lengths (in Å) and angles (in degrees) at PBE0/AVTZ.

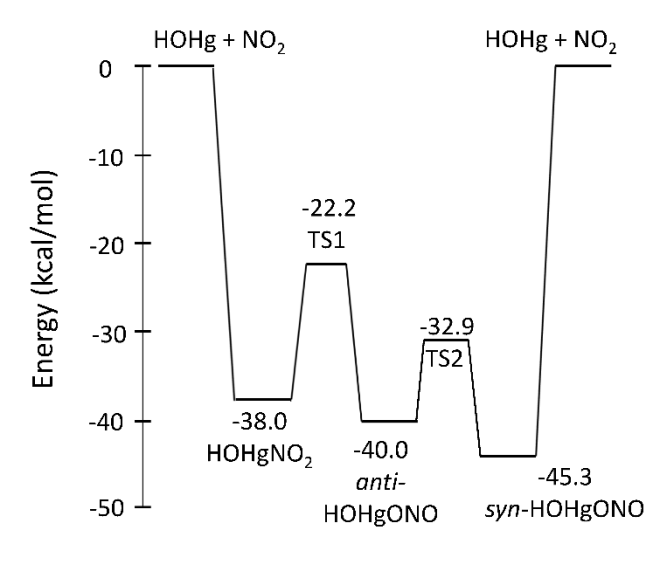


Figure 3: Potential Energy Profile for HOHg• + NO₂ at CCSD(T)//PBE0/AVTZ. The two conformers of *syn*-HOHgONO are treated as one species here.

At 298 K, 99.98% of the products of the HOHg• + NO₂ reaction will exist as *syn*-HOHgONO. RRKM/Master Equation calculations in MultiWell^{69–71} and MESMER⁷² indicate that at conditions typical of the tropopause (220 K and 0.1 atm), more than 90% of HOHgNO₂ will promptly (~20 ps) isomerize to the HOHgONO conformers, and the anti conformer is transformed to the syn conformer in less than 1 μs. However, under these conditions, the lifetime for transforming the small remaining fraction of thermalized HOHgNO₂ to *syn*-HOHgONO is about 1000 sec. By contrast, at 1 atm and 298 K, the system only takes about 1 second to reach equilibrium. For modeling purposes, it seems reasonable to treat *syn*-HOHgONO as the sole product of addition of NO₂ to HOHg•.

HOHg-Y bond energies (D_0) are listed in Table 4. Note that Guzman and Bozzelli⁵⁹ obtained 56.2 kcal/mole (at 298 K) for the HOHg-OBr bond enthalpy, which is in good agreement with our value of $D_0 = 56.7$ kcal/mole. Figure 4 shows that values of D_0 for each HOHg-Y compound nearly match those for the corresponding BrHg-Y.²¹ Regression analysis shows them to correlate as:

$$D_0(HOHg-Y) = 1.008 \times D_0(HOHg-Y) + 1.2 \text{ kcal/mole}$$
 (14)

with $R^2 = 0.996$. Note two methodological differences between these two studies: structures were obtained with PBE0 for HOHgY and B3LYP for BrHgY; also, the BrHg-Y calculations correlated more orbitals than is proper for the AVTZ basis set. For higher level studies of the structures and energetics of BrHgY compounds, see references 24 and 62.

Y	PBE0	CCSD(T)//PBE0
-OBr	51.9	56.7
-ONO (syn-cis)	39.0	45.3
-ONO (syn-trans)	38.8	45.2
-ONO (anti)	33.0	40.0
-NO ₂	35.3	38.0
-OOH	38.6	44.1
-OOCH ₃	38.1	44.1
-NO	11.2	11.0
-O ₂	8.6	9.3

Table 4: HOHg-Y bond energies (kcal/mole at 0 K) at PBE0/AVTZ and CCSD(T)//PBE0/AVTZ.

Although we previously discussed the possibility that BrHg• would react with organic peroxy radicals (ROO•) to form BrHgOOR,²² no studies of this reaction have been published. Here we find that the HOHg-OOCH₃ bond energy to be the same as that for HOHg-OOH (see Table 4). This tends to support our prior speculations on the stability of BrHgOOR.

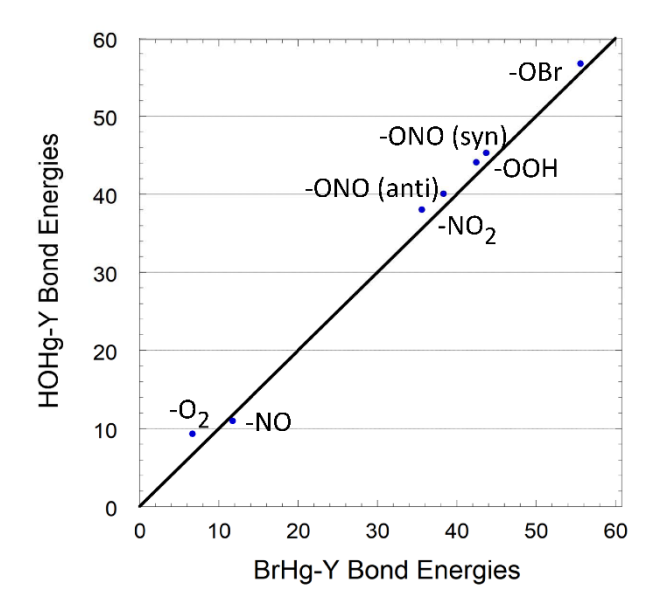


Figure 4: HOHg-Y bond energies (kcal/mole at CCSD(T)//PBE0/AVTZ) from this work vs. BrHg-Y bond energies (CCSD(T)//B3LYP/AVTZ) from Ref 21. The diagonal line corresponds to equal bond energies in the two classes of molecules.

In a previous paper²⁴ we argued that BrHgNO thermally dissociates faster than it could undergo other reactions. Given that HOHgNO and BrHgNO possess essentially the same Hg-N bond energy, we conclude that the main fate of HOHgNO is dissociation. The same argument holds for *individual* molecules of BrHgOO• and HOHgOO•. However, the abundance of O₂ means that, at any given time, small fractions of BrHg• and HOHg• will exist as BrHgOO• and HOHgOO•, respectively. Calculations are needed to obtain more precise values of Hg-O₂ bond energies in these radicals and to investigate their reactions in the atmosphere.

Having dealt with the reactions of HOHg• with abundant radicals, let us consider how HOHg• might react with VOCs: by abstraction of hydrogen atoms or addition to sp²-hybridized carbon atoms. We previously reported that BrHg• will not abstract hydrogen atoms from volatile organic compounds (VOCs). These reactions are thermodynamically disfavored due to the weakness of the BrHg-H bond ($D_0 = 73 \pm 3 \text{ kcal/mole}$). Here we report that the isodesmic reaction:

$$HOHgH + BrHg \rightarrow HOHg + BrHgH$$
 (15)

possesses an enthalpy of reaction (at 0 K) of ± 3.5 kcal/mole at CCSD(T)//PBE0/AVTZ. This means that the HOHg-H bond energy amounts to only 76 ± 3 kcal/mole, which is much weaker than C-H and O-H bonds in VOCs. Consequently, we do not expect HOHg• to abstract hydrogen atoms from VOCs.

Our study⁷³ of the BrHg• + CH₂=CH₂ reaction showed that, like OH + CH₂=CH₂, this reaction proceeds by a barrierless formation of a van der Waals complex, which then passes over a transition state to form BrHgCH₂CH₂•. Figure 5 depicts the potential energy profile for the analogous HOHg• + ethylene system at PBE0/AVTZ. Like the analogous BrHg• + ethylene reaction, this reaction is roughly thermoneutral. At the PBE0/AVTZ level of theory, we find that, as compared to the BrHg• + CH₂=CH₂ reaction, the transition state and reaction products in the HOHg• + CH₂=CH₂ system are both slightly higher in energy relative to reactants (by 1.4 and 3.2 kcal/mole). As we showed, the weakness of the BrHg-CH₂CH₂• bond means that this radical will dissociate before undergoing any bimolecular collisions.⁷³ Given the higher barrier and lesser stability of the products in the HOHg• + CH₂=CH₂ reaction, we suggests that HOHg• addition to alkenes will be very inefficient.

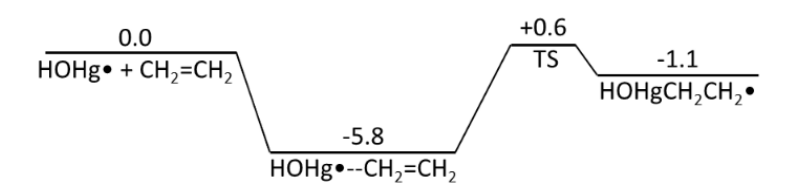


Figure 5. Potential energy profile for HOHg• + CH₂=CH₂ at PBE0/AVTZ.

Proposed Mechanism and Rate Constants for the OH-Initiated oxidation of Hg(0). Based on the similarity of the BrHg-Y and HOHg-Y bond energies, their formation reactions will likely possess similar pressure- and temperature-dependent rate constants, k([M],T). For purposes of modeling, we suggest assuming that the values are identical. We fit the rate constants reported by Jiao and Dibble²² for BrHg• + NO₂ and BrHg• + HOO to the Troe expression:⁷⁴

$$k([M],T) = \left(\frac{k_0(T)[M]}{1 + \frac{k_0(T)[M]}{k_{\infty}(T)}}\right) F_c^{\gamma}$$
(16)

where F_c is assumed to be 0.6, k_0 is the rate constant in the low-pressure limit, k_{∞} is the rate constant in the high-pressure limit, and γ is defined by:

$$\gamma = \left\{ 1 + \left[log_{10} \left(\frac{k_0(T)[M]}{k_{\infty}(T)} \right) \right]^2 \right\}^{-1}$$
(17)

The resulting values of $k_0(T)$ and $k_{\infty}(T)$ are listed in Table 5. Consistent with Horowitz et al.,²³ we assume the rate constant for HOHg• + •Y takes on one value for Y = •NO₂ and another value for all other •Y.

It has been shown that BrHg-OX bond energies vary rather little between X=Cl, Br, and I;^{62,59} Guzman and Bozzelli showed this for HOHg-OX ⁵⁹ Consequently, we include HOHg• reaction with ClO and IO in the mechanism in Table 5. In a previous paper, we demonstrated the

existence of BrHgXO compounds (X=Cl, Br, I) that were 26-28 kcal/mole less stable than the corresponding BrHgOX species.⁶² So we confidently predict that the corresponding HOHgXO compounds exist and are similarly less stable than their HOHgOX counterparts.

Table 5. Mechanism and rate constants for the OH-initiated oxidation of Hg(0). The reaction $OH + Hg + M \leftrightarrows HOHg \cdot + M$ is assumed to be in the low-pressure limit.

Reaction	Rate Constant ^{a, b}
$OH + Hg + M \rightarrow HOHg \bullet + M$	$3.34 \times 10^{-33} \mathrm{e}^{+43/\mathrm{T}}$
$HOHg \cdot + M \rightarrow OH + Hg + M$	$1.22 \times 10^{-9} \mathrm{e}^{-5720/\mathrm{T}}$
$\text{HOHg} \bullet + \text{NO}_2 \xrightarrow{\text{M}} \textit{syn-HOHgONO}$	$k_0(T) = 7.1 \times 10^{-29} (\text{T/300})^{-4.5}$ $k_{\infty}(T) = 1.2 \times 10^{-10} (\text{T/300})^{-1.9}$
HOHg• + •Y \xrightarrow{M} HOHgY •Y = (HOO, CH ₃ OO, ClO, BrO, etc.)	$k_0(T) = 2.3 \times 10^{-29} (\text{T}/300)^{-4.4}$ $k_{\infty}(T) = 6.9 \times 10^{-11} (\text{T}/300)^{-2.4}$

a) k_1 and both values of k_0 possess units of cm⁶ molecule⁻² sec⁻¹. k_{-1} and k_{∞} are in cm³ molecule⁻¹ sec⁻¹.

Calvert and Lindberg¹² buttressed their analysis of the experiment of Pal and Ariya¹⁰ with kinetic modeling. We carried out simulations based on their model, after updating the mercury chemistry and adding OH reaction with isopropylnitrite and multiple generations of reactions of the products. We find that the fate of HOHg• under the experimental conditions of Pal and Ariya is almost entirely reaction with NO₂ rather than dissociation. Analysis of the extent of formation of NO₂ in the experiments of Sommar et al.⁸ reaches the same conclusion. Details of both analyses may be found in the Supporting Information.

Global Modeling of Oxidation of Gaseous Elemental Mercury We added the above mechanism of OH-initiated oxidation of elemental mercury to the GEOS-Chem global chemistry and transport model⁷⁵ to quantify its atmospheric efficiency and calculate its impact on global atmospheric Hg. We simulated both OH- and Br-initiated oxidation of elemental mercury using GEOS-Chem version 12.3.1.76 The GEOS-Chem model simulates concentrations of the relevant oxidant radical species (OH, Br, Cl, NO₂, HO₂, BrO, ClO, etc.), and we added mercury redox chemistry to this model's standard simulation. Organic peroxy radicals were not included as reactants with BrHg• or HOHg•. We simulated Hg concentrations for the years 2013-2015 with 4°x5° horizontal resolution and 47 vertical levels, using emissions and land surface flux boundary conditions taken from Horowitz et al.²³ As in that work, we coupled our atmospheric simulation to the MITgcm ocean Hg simulation.⁷⁷ Horowitz et al. considered Hg(0) oxidation by Br and Cl atoms in the gas phase and by OH(aq), O3(aq), and HOCl(aq) in cloudwater. They found that gas-phase oxidation by Br atoms accounted for 97% of the global formation of Hg(II).

Gas-phase OH-initiated Hg oxidation was added as defined in Table 5. Other oxidation pathways were as in Horowitz et al. but the pressure and temperature dependence of the second stage of Br-initiated oxidation was changed to reflect the corresponding Troe expressions above. Following Saiz-Lopez et al.,²⁷ we used the photolysis cross sections of BrHgY species to

b) $k_0(T)$ and $k_{\infty}(T)$ are used in the Troe expression (Eqns. 16 and 17 in the text) to get k([M],T)

calculate photolysis rate constants using the Fast-JX code implemented in GEOS-Chem. Rhotolysis of BrHgY is assumed to produce BrHg• + •Y with the exception of BrHgONO, which leads to BrHgOH via BrHgO•. We assume that, for each BrHgY species, the analogous HOHgY species has the same photolysis properties. While the substitution of OH for Br should cause shifts in the absorption spectra and corresponding differences in photolysis lifetimes, this effect would have to be large to affect our overall conclusions. By treating the photo-reduction of BrHgY and HOHgY identically, our simulations isolate the impact of the OH-initiated oxidation as described in this work.

Figure 6 shows the annually averaged fraction of HOHg• (top) and BrHg• (bottom) that goes on to form Hg(II) species. OH-initiated oxidation is highly inefficient at ground level. At all surface locations in the simulation, less than 15% of HOHg• goes on to form Hg(II) instead of decomposing to Hg(0). For most of the globe, this fraction is less than 5%, but the Eastern United States, Europe, and Eastern China show elevated fractions due to the presence of higher quantities of second-stage oxidants such as NO₂. In contrast to oxidation via OH, Br-initiated oxidation is more than 70% efficient at ground level for most of the Northern Hemisphere. Since thermal decomposition of HOHg• competes with the second stage of oxidation, the efficiency of converting HOHg• to Hg(II) increases with increasing altitude.

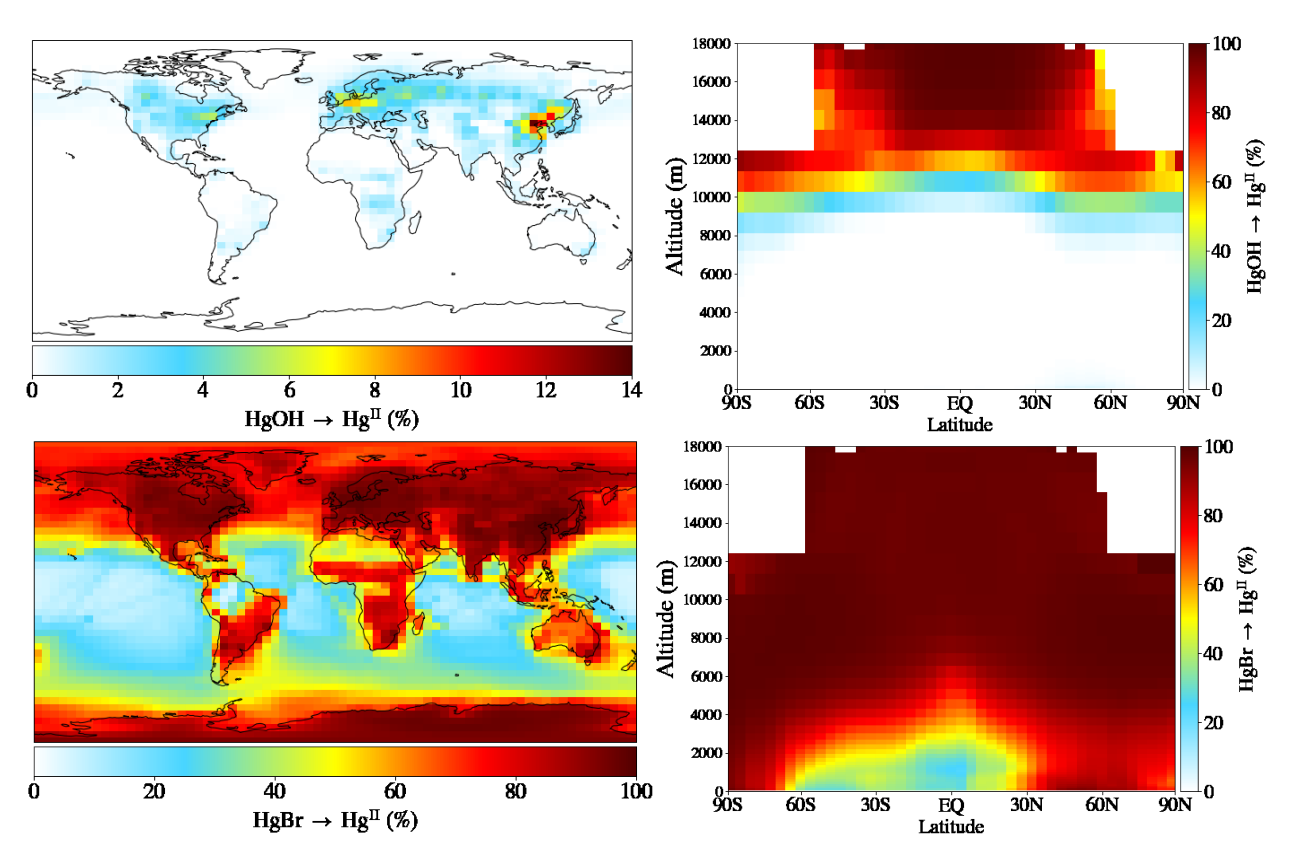


Figure 6. Annually averaged percent of HOHg• (top) and BrHg• (bottom) going on to form Hg(II) compounds. (Left) spatial variation at ground level for the entire globe. (Right) variation with altitude and latitude averaged over longitude.

Because of the inefficiency of OH-initiated oxidation, adding OH-initiated oxidation to a model that already includes Br-initiated oxidation has a small effect on concentrations of total gaseous mercury (TGM, the sum of gas-phase Hg(0) and Hg(II)). In highly polluted areas (North America, Europe and East Asia) concentrations of reactive gaseous mercury (Hg(II) (g), aka RGM) increase by up to 5%. Outside of these areas, OH-initiated oxidation has effectively no *insitu* effect on RGM or TGM concentrations. However, the addition of OH-initiated oxidation near sources of Hg emissions decreases the atmospheric lifetime of these emissions, and decreases global TGM mass by 2%. Figure 7 shows the fraction of total Hg(II) formation originating from Hg + OH. In the most polluted regions, it can reach up to 83%, but is less than 1% for the majority of the globe at ground level. Globally, Hg + OH contributes 0.5% of Hg(II) formation.

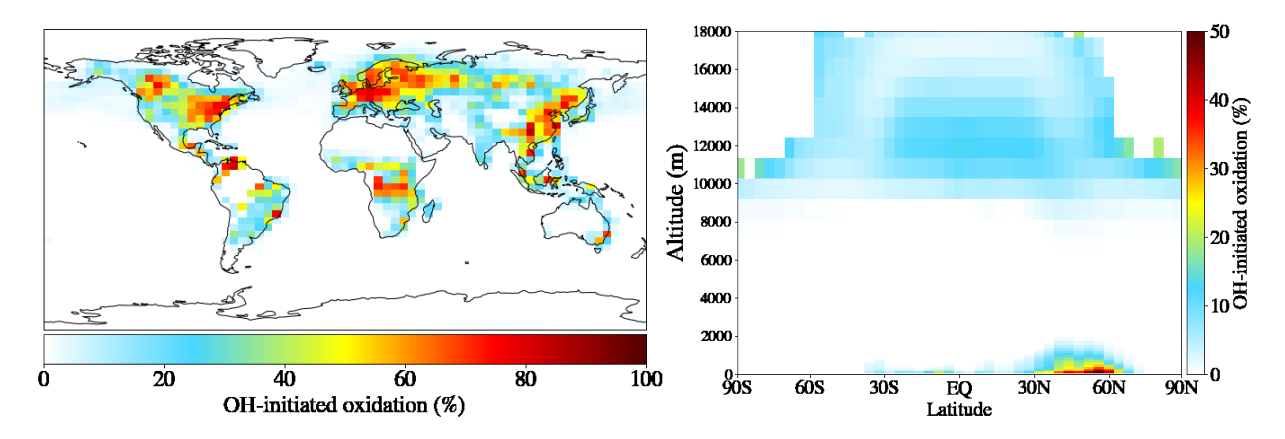


Figure 7. Annually averaged percent of total oxidation initiated by OH. (Left) spatial variation at ground level for the entire globe. (Right) variation with altitude and latitude averaged over longitude.

Recently, Saiz-Lopez et al.²⁶ suggested that photolysis of HOHg• and BrHg• could be an important atmospheric reduction process, and that photolysis occurs somewhat more rapidly for BrHg• than HOHg•. Inclusion of this effect would not make OH important for global oxidation of GEM.

CONCLUSIONS AND FURTHER WORK

We have presented a mechanism and rate constants for the two-step oxidation of Hg(0) to Hg(II) initiated by OH radical in the gaseous atmosphere. We implemented these results into the GEOS-Chem global atmospheric Hg model. The resulting simulations predict that the main pathway for Hg(0) oxidation to Hg(II) occurs through the initial Hg + Br reaction. We find that the Hg + OH pathway contributes <1% of the conversion of Hg(0) to Hg(II), globally, but up to 83% in polluted regions.

Experimental investigation of $k_1([M],T)$ using direct monitoring of OH radical by LIF only led to an upper limit to $k_1(298)$. Under those experimental conditions, the lifetime for loss of OH

by processes other than reaction with Hg(0) was about 5 ms. Our results indicate that $HOHg \bullet$ possesses a lifetime of 7 ms at 298 K and 1 atm of air. Consequently, we suggest that the fast regeneration of OH from dissociation of $HOHg \bullet$ does not present an insuperable obstacle to use of LIF to measure k_1 .

Experimental measurements of $k_{-1}([M],T)$ would improve the reliability of our model of HOHg• formation and dissociation. Note that Saiz-Lopez et al.²⁶ reported that HOHg• will be photolyzed with a global lifetime of ~100 seconds, but experiments are needed to verify their computed photo-absorption cross-sections. Experimentally determining either $k_{-1}([M],T)$ or these photo-absorption cross-section will be a challenge, since, to date, HOHg• has only been detected in a single laboratory study, and only in aqueous solution.⁸⁰

Except for the value of the bimolecular rate constant, $k_1(T, 1 \text{ atm})$, over the range 283 K $\leq T \leq$ 353 K, our entire mechanism is based on computational chemistry and chemical insight. In particular, the rate constants for BrHg• reaction with NO₂ and HOO• used for the HOHg• + •Y reactions are, themselves, the result of calculations that have yet to be verified by experiment. Validation or improvement of the HOHg• + •Y rate constants is a high-priority item for improving the reliability of our mechanism.

Previously, Saiz-Lopez et al. reported relativistic CASPT2 calculations indicating that photolysis of BrHgY compounds occurs very rapidly in the atmosphere,²⁷ and Lam et al. affirmed this for BrHgONO using non-relativistic EOM-CCSD calculations.²⁵ No laboratory experimental data has been reported for any BrHgY or HOHgY compound, and the spectra of HOHgY compounds has not been computed. These compounds are important targets for future studies, since atmospheric modelers need to know their spectra, photolysis quantum yields, and whether their photolysis leads to photo-reduction.

ASSOCIATED CONTENT

Supporting Information

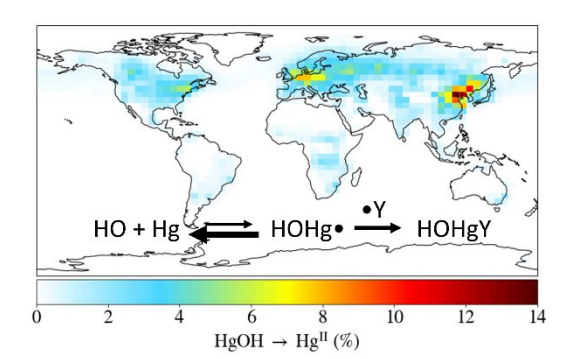
The Supporting Information is available free of charge on the ACS Publications website at DOI: ____. Absolute energies of all species at all levels of theory along with zero-point energies, Cartesian coordinates, rotational constants, and vibrational frequencies; values of the T1 diagnostic; thermochemical data; kinetic analyses of the experiments of reference 8; Figures showing additional model results (PDF); kinetic model for analysis of experiments of reference 10 (Excel).

ACKNOWLEDGEMENTS

The work at SUNY-ESF was partially supported by the National Science Foundation under award 1609848. Some computations were carried out using resources of the Extreme Science and Engineering Discovery Environment (XSEDE), which is supported by National Science Foundation Grant Number ACI-1053575; specifically, we used Bridges at the Pittsburgh

Supercomputing Center (PSC) and Comet at the San Diego Supercomputer Center (SDSC). We also thank Huiting Mao for helpful discussions and Khoa T. Lam for advice on calculations. The work at Harvard was supported by the US National Science Foundation Atmospheric Chemistry Program under award AGS-1643217.

TOC Graphic



REFERENCES

- (1) Driscoll, C. T.; Mason, R. P.; Chan, H. M.; Jacob, D. J.; Pirrone, N. Mercury as a Global Pollutant: Sources, Pathways, and Effects. **2013**, *47*, 4967–4983.
- (2) Minimata Convention on Mercury. 2013.http://www.mercuryconvention.org
- (3) Zhang, L.; Wang, S.; Wu, Q.; Wang, F.; Lin, C.-J.; Zhang, L.; Hui, M.; Yang, M.; Su, H.; Hao, J. Mercury Transformation and Speciation in Flue Gases from Anthropogenic Emission Sources: A Critical Review. *Atmos. Chem. Phys.* 2016, 16, 2417–2433.
- (4) Schroeder, W. H.; Munthe, J. Atmospheric Mercury—An Overview. *Atmos. Environ.* **1998**, *32*, 809–822.
- (5) Lin, C. J.; Pongprueksa, P.; Bullock, R. O.; Lindberg, S. E.; Pehkonen, S. O.; Jang, C.; Braverman, T.; Ho, T. C. Scientific Uncertainties in Atmospheric Mercury Models II: Sensitivity Analysis in the CONUS Domain. *Atmos. Environ.* **2007**, *41*, 6544–6560.
- (6) Gustin, M. S.; Amos, H. M.; Huang, J.; Miller, M. B.; Heidecorn, K. Measuring and Modeling Mercury in the Atmosphere: A Critical Review. *Atmos. Chem. Phys.* **2015**, *15*, 5697–5713.
- (7) Gencarelli, C. N.; Bieser, J.; Carbone, F.; De Simone, F.; Hedgecock, I. M.; Matthias, V.; Travnikov, O.; Yang, X.; Pirrone, N. Sensitivity Model Study of Regional Mercury Dispersion in the Atmosphere. *Atmos. Chem. Phys.* **2017**, *17*, 627–643.
- (8) Sommar, J.; Gårdfeldt, K.; Strömberg, D.; Feng, X. A Kinetic Study of the Gas-Phase Reaction between the Hydroxyl Radical and Atomic Mercury. *Atmos. Environ.* **2001**, *35*, 3049–3054.
- (9) Bauer, D.; D'Ottone, L.; Campuzano-Jost, P.; Hynes, A. . Gas Phase Elemental Mercury: A Comparison of LIF Detection Techniques and Study of the Kinetics of Reaction with the Hydroxyl Radical. *J. Photochem. Photobiol. A Chem.* **2003**, *157*, 247–256.
- (10) Pal, B.; Ariya, P. A. Gas-Phase HO-Initiated Reactions of Elemental Mercury: Kinetics, Product Studies, and Atmospheric Implications. *Environ. Sci. Technol.* **2004**, *38*, 5555–5566.
- (11) Goodsite, M. E. Plane, J. M. C.; Skov, H. A Theoretical Study of the Oxidation of Hg⁰ to HgBr₂ in the Troposphere. *Environ. Sci. Technol.* **2004**, *38*, 1772–1776.
- (12) Calvert, J. G.; Lindberg, S. E. Mechanisms of Mercury Removal by O₃ and OH in the Atmosphere. *Atmos. Environ.* **2005**, *39*, 3355–3367.
- (13) Travnikov, O.; Angot, H.; Artaxo, P.; Bencardino, M.; Bieser, J.; D'Amore, F.; Dastoor, A.; De Simone, F.; Diéguez, M. D. C.; Dommergue, A.; et al. Multi-Model Study of Mercury Dispersion in the Atmosphere: Atmospheric Processes and Model Evaluation. *Atmos. Chem. Phys.* **2017**, *17*, 5271–5295.
- (14) Bullock, O. R.; Brehme, K. A. Atmospheric Mercury Simulation Using the CMAQ Model: Formulation Description and Analysis of Wet Deposition Results. *Atmos. Environ.* **2002**, *36*, 2135–2146.

- (15) Jung, G.; Hedgecock, I. M.; Pirrone, N. ECHMERIT V1.0 a New Global Fully Coupled Mercury-Chemistry and Transport Model. *Geosci. Model Dev.* **2009**, *2*, 175–195.
- (16) Shepler, B. C.; Peterson, K. A. Mercury Monoxide: A Systematic Investigation of Its Ground Electronic State. *J. Phys. Chem. A* **2003**, *107*, 1783–1787.
- (17) Filatov, M.; Cremer, D. Revision of the Dissociation Energies of Mercury Chalcogenides-Unusual Types of Mercury Bonding. *Chemphyschem* **2004**, *5*, 1547–1557.
- (18) Tossell, J. A. Calculation of the Energetics for the Oligomerization of Gas Phase HgO and HgS and for the Solvolysis of Crystalline HgO and HgS. *J. Phys. Chem. A* **2006**, *110*, 2571–2578.
- (19) Peterson, K. A.; Shepler, B. C.; Singleton, J. M. The Group 12 Metal Chalcogenides: An Accurate Multireference Configuration Interaction and Coupled Cluster Study. *Mol. Phys.* **2007**, *105*, 1139–1155.
- (20) Cremer, D.; Kraka, E.; Filatov, M. Bonding in Mercury Molecules Described by the Normalized Elimination of the Small Component and Coupled Cluster Theory. *ChemPhysChem* **2008**, *9*, 2510–2521.
- (21) Dibble, T. S.; Zelie, M. J.; Mao, H. Thermodynamics of Reactions of ClHg and BrHg Radicals with Atmospherically Abundant Free Radicals. *Atmos. Chem. Phys.* **2012**, *12*, 10271–10279.
- (22) Jiao, Y.; Dibble, T. S. First Kinetic Study of the Atmospherically Important Reactions BrHg + NO₂ and BrHg + HOO. *Phys. Chem. Chem. Phys.* **2017**, *19*, 1826–1838.
- (23) Horowitz, H. M.; Jacob, D. J.; Zhang, Y.; Dibble, T. S.; Slemr, F.; Amos, H. M.; Schmidt, J. A.; Corbitt, E. S.; Marais, E. A.; Sunderland, E. M. A New Mechanism for Atmospheric Mercury Redox Chemistry: Implications for the Global Mercury Budget. *Atmos. Chem. Phys.* **2017**, *17*, 6353–6371.
- (24) Jiao, Y.; Dibble, T. S. Quality Structures, Vibrational Frequencies, and Thermochemistry of the Products of Reaction of BrHg with NO₂, HO₂, ClO, BrO, and IO. *J. Phys. Chem. A* **2015**, *119*, 10502–10510.
- (25) Lam, K. T.; Wilhelmsen, C. J.; Schwid, A. C.; Jiao, Y.; Dibble, T. S. Computational Study on the Photolysis of BrHgONO and the Reactions of BrHgO• with CH₄, C₂H₆, NO, and NO₂: Implications for Formation of Hg(II) Compounds in the Atmosphere. *J. Phys. Chem. A* **2019**, *123*, 1637–1647.
- (26) Saiz-Lopez, A.; Ulises Acuña, A.; Trabelsi, T.; Carmona-García, J.; Z. Dávalos, J.; Rivero, D.; A. Cuevas, C.; E. Kinnison, D.; P. Sitkiewicz, S.; Roca-Sanjuán, D.; et al. Gas-Phase Photolysis of Hg(I) Radical Species: A New Atmospheric Mercury Reduction Process. *J. Am. Chem. Soc.* **2019**, *141*, 8698–8702.
- (27) Saiz-Lopez, A.; Sitkiewicz, S. P.; Roca-Sanjuán, D.; Oliva-Enrich, J. M.; Dávalos, J. Z.; Notario, R.; Jiskra, M.; Xu, Y.; Wang, F.; Thackray, C. P.; et al. Photoreduction of Gaseous Oxidized Mercury Changes Global Atmospheric Mercury Speciation, Transport and Deposition. *Nat. Commun.* **2018**, *9*, 4796.

- (28) Sun, G.; Sommar, J.; Feng, X.; Lin, C.-J.; Ge, M.; Wang, W.; Yin, R.; Fu, X.; Shang, L. Mass-Dependent and -Independent Fractionation of Mercury Isotope during Gas-Phase Oxidation of Elemental Mercury Vapor by Atomic Cl and Br. *Environ. Sci. Technol.* **2016**, 50, 9232–9241.
- (29) Dibble, T. S.; Zelie, M. J.; Mao, H. Thermodynamics of Reactions of ClHg and BrHg Radicals with Atmospherically Abundant Free Radicals. *Atmos. Chem. Phys.* **2012**, *12*, 10271–10279.
- (30) Frisch, M. J.; Trucks, G. W.; Schlegel, H. B.; Scuseria, G. E.; Robb, M. A.; Cheeseman, J. R.; Scalmani, G.; Barone, V.; Petersson, G. A.; Nakatsuji, H.; et al. Gaussian 09, Revision D.01. Wallingford CT 2016.
- (31) Frisch, M. J.; Trucks, G. W.; Schlegel, H. B.; Scuseria, G. E.; Robb, M. A.; Cheeseman, J. R.; Scalmani, G.; Barone, V.; Petersson, G. A.; Nakatsuji, H. et al. Gaussian 16, Rev. A. Gaussian, Inc.: Wallingford CT 2016.
- (32) Kendall, R. A.; Dunning, T. H.; Harrison, R. J. Electron Affinities of the First-row Atoms Revisited. Systematic Basis Sets and Wave Functions. *J. Chem. Phys.* **1992**, *96*, 6796–6806.
- (33) Peterson, K. A.; Figgen, D.; Goll, E.; Stoll, H.; Dolg, M. Systematically Convergent Basis Sets with Relativistic Pseudopotentials. II. Small-Core Pseudopotentials and Correlation Consistent Basis Sets for the Post-d Group 16–18 Elements. *J. Chem. Phys.* **2003**, *119*, 11113.
- (34) Figgen, D.; Rauhut, G.; Dolg, M.; Stoll, H. Energy-Consistent Pseudopotentials for Group 11 and 12 Atoms: Adjustment to Multi-Configuration Dirac-Hartree-Fock Data. *Chem. Phys.* **2005**, *311*, 227–244.
- (35) Peterson, K. A.; Shepler, B. C.; Figgen, D.; Stoll, H. On the Spectroscopic and Thermochemical Properties of ClO, BrO, IO, and Their Anions. *J. Phys. Chem. A* **2006**, *110*, 13877–13883.
- (36) Peterson, K. A.; Puzzarini, C. Systematically Convergent Basis Sets for Transition Metals. II. Pseudopotential-Based Correlation Consistent Basis Sets for the Group 11 (Cu, Ag, Au) and 12 (Zn, Cd, Hg) Elements. *Theor. Chem. Acc.* **2005**, *114*, 283–296.
- (37) Tajti, A.; Szalay, P. G.; Császár, A. G.; Kállay, M.; Gauss, J.; Valeev, E. F.; Flowers, B. A.; Vázquez, J.; Stanton, J. F. HEAT: High Accuracy Extrapolated Ab Initio Thermochemistry. *J. Chem. Phys.* **2004**, *121*, 11599–11613.
- (38) Bomble, Y. J.; Vázquez, J.; Kállay, M.; Michauk, C.; Szalay, P. G.; Császár, A. G.; Gauss, J.; Stanton, J. F. High-Accuracy Extrapolated Ab Initio Thermochemistry. II. Minor Improvements to the Protocol and a Vital Simplification. *J. Chem. Phys.* **2006**, *125*, 064108.
- (39) Stanton, J. F.; Gauss, J.; Harding, M. E.; Szalay, P. G. CFOUR, Coupled-Cluster Techniques for Computational Chemistry. http://www.cfour.de
- (40) Kállay, M.; Rolik, Z.; Csontos, J.; Nagy, P.; Samu, G.; Mester, D.; Ladjánszki, I.; Szegedy, L.; Ladóczki, B.; Petrov, K.; et al. MRCC, a Quantum Chemical Program Suite.

- (41) Aquilante, F.; Autschbach, J.; Carlson, R. K.; Chibotaru, L. F.; Delcey, M. G.; De Vico, L.; Fernandez Galván, I.; Ferré, N.; Frutos, L. M.; Gagliardi, L.; et al. Molcas 8: New Capabilities for Multiconfigurational Quantum Chemical Calculations across the Periodic Table. *J. Comput. Chem.* **2016**, *37*, 506–541.
- (42) Cheng, L.; Gauss, J. Analytic Energy Gradients for the Spin-Free Exact Two-Component Theory Using an Exact Block Diagonalization for the One-Electron Dirac Hamiltonian. *J. Chem. Phys.* **2011**, *135*, 084114.
- (43) Peterson, K. A.; Dunning, T. H. Accurate Correlation Consistent Basis Sets for Molecular Core–Valence Correlation Effects: The Second Row Atoms Al–Ar, and the First Row Atoms B–Ne Revisited. *J. Chem. Phys.* **2002**, *117*, 10548–10560.
- (44) Peterson, K. A.; Woon, D. E.; Dunning, T. H. Benchmark Calculations with Correlated Molecular Wave Functions. IV. The Classical Barrier Height of the H+H2→H₂+H Reaction. *J. Chem. Phys.* **1994**, *100*, 7410–7415.
- (45) Feller, D.; Peterson, K. A. Re-Examination of Atomization Energies for the Gaussian-2 Set of Molecules. *J. Chem. Phys.* **1999**, *110*, 8384–8396.
- (46) Noga, J.; Bartlett, R. J. The Full CCSDT Model for Molecular Electronic Structure. *J. Chem. Phys.* **1987**, *86*, 7041.
- (47) Scuseria, G. E.; Schaefer, H. F. A New Implementation of the Full CCSDT Model for Molecular Electronic Structure. *Chem. Phys. Lett.* **1988**, *152*, 382–386.
- (48) Bomble, Y. J.; Stanton, J. F.; Kállay, M.; Gauss, J. Coupled-Cluster Methods Including Noniterative Corrections for Quadruple Excitations. *J. Chem. Phys.* **2005**, *123*, 054101.
- (49) Kállay, M.; Gauss, J. Approximate Treatment of Higher Excitations in Coupled-Cluster Theory. *J. Chem. Phys.* **2005**, *123*, 214105.
- (50) Malmqvist, P. Å.; Roos, B. O. The CASSCF State Interaction Method. *Chem. Phys. Lett.* **1989**, *155*, 189–194.
- (51) Malmqvist, P. Å.; Roos, B. O.; Schimmelpfennig, B. The Restricted Active Space (RAS) State Interaction Approach with Spin-Orbit Coupling. *Chem. Phys. Lett.* **2002**, *357*, 230–240.
- (52) Roos, B. O.; Malmqvist, P. A. Relativistic Quantum Chemistry: The Multiconfigurational Approach. *Phys. Chem. Chem. Phys.* **2004**, *6*, 2919–2927.
- (53) Ghigo, G.; Roos, B. O.; Malmqvist, P.-Å. A Modified Definition of the Zeroth-Order Hamiltonian in Multiconfigurational Perturbation Theory (CASPT2). *Chem. Phys. Lett.* **2004**, *396*, 142–149.
- (54) Heß, B. A.; Marian, C. M.; Wahlgren, U.; Gropen, O. A Mean-Field Spin-Orbit Method Applicable to Correlated Wavefunctions. *Chem. Phys. Lett.* **1996**, *251*, 365–371.
- (55) Roos, B. O.; Lindh, R.; Malmqvist, P. Å.; Veryazov, V.; Widmark, P. O. New Relativistic ANO Basis Sets for Transition Metal Atoms. *J. Phys. Chem. A* **2005**, *109*, 6575–6579.
- (56) Roos, B. O.; Lindh, R.; Malmqvist, P. Å.; Veryazov, V.; Widmark, P. O. Main Group

- Atoms and Dimers Studied with a New Relativistic ANO Basis Set. J. Phys. Chem. A **2004**, 108 (15), 2851–2858.
- (57) Brown, J. M.; Kerr, C. M. L.; Wayne, F. D.; Evenson, K. M.; Radford, H. E. The Far-Infrared Laser Magnetic Resonance Spectrum of the OH Radical. *J. Mol. Spectrosc.* **1981**, 86 (2), 544–554.
- (58) Ezarfi, N.; Touimi Benjelloun, A.; Sabor, S.; Benzakour, M.; Mcharfi, M. Theoretical Investigations of Structural, Thermal Properties and Stability of the Group 12 Metal M(XH) Isomers in Atmosphere: M = (Zn, Cd, Hg) and XH = (OH, SH). *Theor. Chem. Acc.* **2019**, *138*, 109.
- (59) Guzman, F. J.; Bozzelli, J. Thermodynamics of OHgX, XHgOH, XHgOCl, XHgOBr, and HOHgY Gaseous Oxidized Mercury Molecules from Isodesmic, Isogyric, and Atomization Work Reactions (X = Halogen, Y = OH, OCl, OBr). *J. Phys. Chem. A* **2019**, 123, 4452–4464.
- (60) Lee, T. J.; Taylor, P. R. A Diagnostic for Determining the Quality of Single-Reference Electron Correlation Methods. *Int. J. Quantum Chem.* **2009**, *36*, 199–207.
- (61) Harding, M. E.; Vázquez, J.; Ruscic, B.; Wilson, A. K.; Gauss, J.; Stanton, J. F. High-Accuracy Extrapolated Ab Initio Thermochemistry. III. Additional Improvements and Overview. *J. Chem. Phys.* **2008**, *128*, 114111.
- (62) Jiao, Y.; Dibble, T. S. Structures, Vibrational Frequencies, and Bond Energies of the BrHgOX and BrHgXO Species Formed in Atmospheric Mercury Depletion Events. *J. Phys. Chem. A* **2017**, *121* 7976-7985.
- (63) Tossell, J. A. Calculation of the Energetics for Oxidation of Gas-Phase Elemental Hg by Br and BrO. *J. Phys. Chem. A* **2003**, *107*, 7804–7808.
- (64) Chase, M. W., J. NIST-JANAF Thermochemical Tables, 4th Ed., Journal of Physical and Chemical Reference Data Monographs 9; 1998.
- (65) Bakk, I. P.; Benkö, N.; Nyulászi, L. The Effect of Contaminants on the Mercury Consumption of Fluorescent Lamps. *J. Phys. D. Appl. Phys.* **2009**, *42*, 095501.
- (66) Balabanov, N. B.; Peterson, K. A. Mercury and Reactive Halogens: The Thermochemistry of Hg + {Cl₂, Br₂, BrCl, ClO, and BrO}. *J. Phys. Chem. A* **2003**, *107*, 7465–7470.
- (67) Donohoue, D. L.; Bauer, D.; Hynes, A. J. Temperature and Pressure Dependent Rate Coefficients for the Reaction of Hg with Cl and the Reaction of Cl with Cl: A Pulsed Laser Photolysis—Pulsed Laser Induced Fluorescence Study. *J. Phys. Chem. A* **2005**, *109*, 7732–7741.
- (68) Donohoue, D. L.; Bauer, D.; Cossairt, B.; Hynes, A. J. Temperature and Pressure Dependent Rate Coefficients for the Reaction of Hg with Br and the Reaction of Br with Br: A Pulsed Laser Photolysis-Pulsed Laser Induced Fluorescence Study. *J. Phys. Chem. A* **2006**, *110*, 6623–6632.
- (69) Barker, J. R. Multiple-Well, Multiple-Path Unimolecular Reaction Systems. I. MultiWell Computer Program Suite. *Int. J. Chem. Kinet.* **2001**, *33*, 232–245.

- (70) Barker, J. R. Energy Transfer in Master Equation Simulations: A New Approach. *Int. J. Chem. Kinet.* **2009**, *41*, 748–763.
- (71) Barker, J. R.; Nguyen, T. L.; Stanton, J. F.; Aieta, C.; Ceotto, M.; Gabas, F.; Kumar, T. J. D.; Li, C. G. L.; Lohr, L. L.; Maranzana, A.; et al. MultiWell-2019 Software Suite; J. R. Barker, University of Michigan, Ann Arbor, Michigan, USA, 2019 H.
- (72) R. Glowacki, D.; Liang, C.-H.; Morley, C.; J. Pilling, M.; H. Robertson, S. MESMER: An Open-Source Master Equation Solver for Multi-Energy Well Reactions. *J. Phys. Chem. A* **2012**, *116*, 9545–9560.
- (73) Dibble, T. S.; Schwid, A. C. Thermodynamics Limits the Reactivity of BrHg• Radical with Volatile Organic Compounds. *Chem. Phys. Lett.* **2016**, *659*, 289–294.
- (74) Troe, J. Predictive Possibilities of Unimolecular Rate Theory. *J. Phys. Chem.* **1979**, *83*, 114–126.
- (75) Bey, I.; Jacob, D. J.; Yantosca, R. M.; Logan, J. A.; Field, B. D.; Fiore, A. M.; Li, Q.; Liu, H. Y.; Mickley, L. J.; Schultz, M. G. Global Modeling of Tropospheric Chemistry with Assimilated Meteorology: Model Description and Evaluation. *J. Geophys. Res. Atmos. D* **2001**, *106*, 23073–23095.
- (76) International GEOS-Chem User Community. GEOS-Chem 12.3.1. 2019. http://dx.doi.org/10.5281/zenodo.2633278
- (77) Zhang, Y.; Jacob, D. J.; Dutkiewicz, S.; Amos, H. M.; Long, M. S.; Sunderland, E. M. Biogeochemical Drivers of the Fate of Riverine Mercury Discharged to the Global and Arctic Oceans. *Global Biogeochem. Cycles* **2015**, *29*, 854–864.
- (78) Bian, H.; Prather, M. J. Fast-J2: Accurate Simulation of Stratospheric Photolysis in Global Chemical Models. *J. Atmos. Chem.* **2002**, *41*, 281–296.
- (79) Mao, J.; Fan, S.; Jacob, D. J.; Travis, K. R. Radical Loss in the Atmosphere from Cu-Fe Redox Coupling in Aerosols. *Atmos. Chem. Phys.* **2013**, *13*, 509–519.
- (80) Fujita, S.; Horii, H.; Mori, T.; Taniguchi, S. Pulse Radiolysis of Mercuric Oxide in Neutral Aqueous Solutions. *J. Phys. Chem.* **1975**, *79*, 960–964.